

# FPGA Development for the LHCb Vertex Locator Upgrade

Nicholas Mead  
8064141

School of Physics and Astronomy  
University of Manchester

December 24, 2015

## Abstract

Lorem ipsum dolor sit amet, consectetur adipiscing elit. Curabitur blandit purus ut lacus aliquam, a sodales ante sodales. Etiam a elit nunc. Mauris ipsum tellus, ullamcorper et arcu at, cursus malesuada elit. In tempus pellentesque nisi, vel egestas enim cursus tempus. Sed velit urna, luctus sed efficitur sed, laoreet vitae magna. Mauris elementum dignissim lacus vitae tempus. Curabitur laoreet molestie dictum. Donec sit amet auctor nisl.

Duis pellentesque euismod pellentesque. Praesent volutpat tincidunt eros, at faucibus tellus eleifend a. Quisque molestie sed ante sit amet sodales. Duis sed justo quam. Curabitur tellus felis, laoreet et bibendum a, posuere eget nisi. Donec suscipit lacinia porttitor. Aenean posuere sem nibh, et iaculis nisl faucibus eu. Donec ac posuere sapien. Aenean suscipit, nisi eget porttitor viverra, dui sapien vulputate lectus, ut dapibus purus orci nec arcu. Etiam placerat sapien non massa fringilla, et malesuada nibh hendrerit. Vestibulum et porttitor mi. Aliquam turpis velit, rutrum vitae erat at, scelerisque cursus lacus. Praesent libero urna, sodales efficitur eros id, sodales lacinia sem. Pellentesque habitant morbi tristique senectus et netus et malesuada fames ac turpis egestas.



# Contents

24	<b>1 Introduction</b>	<b>1</b>
	1.1 The Standard Model of Particle Physics . . . . .	1
26	1.2 Field Programable Gate Arrays . . . . .	1
	1.3 The LHCb Experiment . . . . .	1
28	1.4 LHCb Upgrade . . . . .	3
	1.4.1 VELO Upgrade . . . . .	3
30	1.4.2 The Role of FPGA's in the VELO Upgrade . . . . .	3
	<b>2 Scrambler</b>	<b>3</b>
32	2.1 Scrambler Options . . . . .	4
	2.2 Cross Checks . . . . .	4
34	2.3 Algorithm Analysis . . . . .	5
	2.3.1 Messurements of the Algorithms . . . . .	5
36	2.3.2 Statistical Predictions . . . . .	6
	2.3.3 Results of Analysis . . . . .	9
38	2.4 Conclusion . . . . .	10
	<b>References</b>	<b>12</b>

# 1 Introduction

## 1.1 The Standard Model of Particle Physics

Central to the modern study of particle physics is the standard model,

$$\begin{aligned}
L_{GWL} = & \sum_f (\bar{\Psi}_f (i\gamma^\mu \partial_\mu - m_f) \Psi_f - e Q_f \bar{\Psi}_f \gamma^\mu \Psi_f A_\mu) + \frac{g}{\sqrt{2}} \sum_i (\bar{a}_L^i \gamma^\mu b_L^i W_\mu^+ + \bar{b}_L^i \gamma^\mu a_L^i W_\mu^-) \\
& + \frac{g}{2x_w} \sum_f \bar{\Psi}_f \gamma^\mu (I_f^3 - 2s_w^2 Q_f - I_6 e_f \gamma_5) \Psi_f Z_\mu - \frac{1}{4} |\partial_\mu A_v - \partial_v A_\mu - ie(W_\mu^- W_v^+ - W_\mu^+ W_v^-)|^2 \\
& - \frac{1}{2} |\partial_\mu W_v^+ - \partial_v W_\mu^+ - ie(W_\mu^+ A_v - W_v^+ A_\mu) + ig' c_w (W_\mu^+ Z_v - W_v^+ Z_\mu)|^2 \\
& - \frac{1}{4} |\partial_\mu Z_v - \partial_v Z_\mu + ig' c_w (W_\mu^- W_v^+ - W_\mu^+ W_v^-)|^2 - \frac{1}{2} M_\eta^2 \eta^2 - \frac{g M_\eta^2}{8 M_W} \eta^3 - \frac{g'^2 M_\eta^2}{32 M_W} \eta^4 \\
& + |M_W W_\mu^+ + \frac{g}{2} \eta W_\mu^+|^2 + \frac{1}{2} |\partial_\mu \eta + i M_Z Z_\mu + \frac{ig}{2c_w} \eta Z_\mu|^2 - \sum_f \frac{gm_f}{2M_W} \bar{\Psi}_f \Psi_f \eta. \quad (1.1)
\end{aligned}$$

The standard model, shown in equation 1.1, is a quantum field theory that describes the fundamental particles and how they interact. While this report does require, or attempt, a detailed understanding the intricate detail of the standard model; the aim of many particle physics experiments is to verify, measure and expand the model. Despite being the current best theory to explain particle interactions, the model is not complete. There are many undescribed phenomena, such as the matter domination in the universe, that require physics beyond the standard model in order to be described. To that end, major international efforts, namely in the form of the Large Hadron Collider, aim to gain further knowledge and understanding of the underlying physics of the universe. [1]

## 1.2 Field Programmable Gate Arrays

## 1.3 The LHCb Experiment

One experiment at the Large Hadron Collider is Large Hadron Collider beauty (LHCb). Located at intersection point 8, LHCb is designed to study rare particle physics phenomena, such as lepton flavour violation and CP violation. The decays studied in the LHCb are via exotic hadronic decays of Bottom or Charm quarks that form short lived hadrons. These hadrons, commonly B mesons, travel in the order of a few cm in the detector before decaying. As such, B meson decays can be identified by decay products that propagate via a secondary vertex.

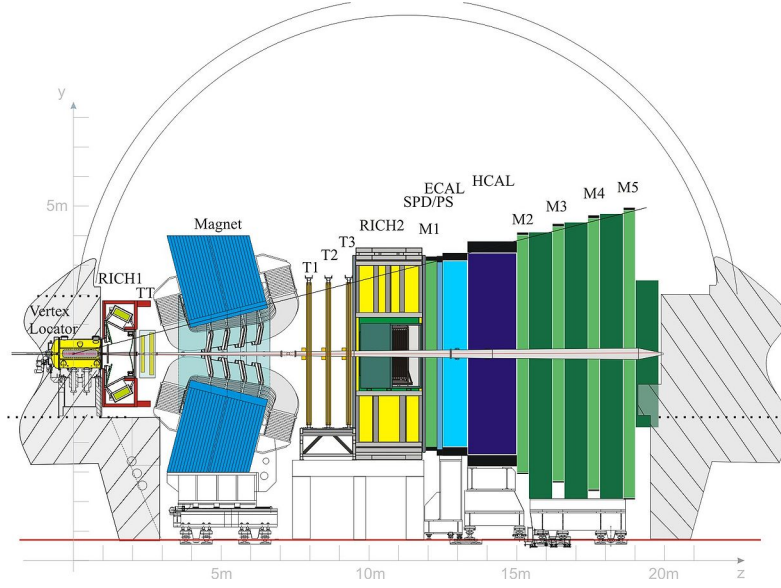


**Figure 1.1:** The LHCb Detector along the bending plane.

As B mesons are light (in comparison to other particles studied in the LHC), the decays products are produced at a shallow angle relative to the beam pipe; this is the driving factor in the design of the experiment. LHCb is a single arm forward spectrometer. Surrounding the point of collision is the Vertex Locator (VELO), this high precision detector uses silicon strips to detect ionising particles as they propagate from a collision and provides the coordinates of the particle in terms of  $R^1$  and  $\phi^2$ . By reconstructing the paths of particles back to the intersection point, it can be identified whether or not the particular decay products are a product of the primary vertex<sup>3</sup>, or a secondary vertex<sup>4</sup>.

The Rich detector, comprised of two subdetectors either side of the magnet, uses cherenkov radiation to deduce the velocity of the particle. The silicon trackers, labeled TT and T1-3 in Figure 1.1, calculate the angle deflection by the magnet. By combining the velocity and angle of deflection, the mass, momentum and energy of the particles can be deduced from simple relativistic kinematics.

The muon detectors, labeled M1-5 in Figure 1.1, are important to detect muons. This is of particular importance on LHCb as muons can be easily misidentified as charged pions, due to their similar mass.

HCAL and ECAL, shown in Figure 1.1, are hadronic and electromagnetic calorimeters respectively. Both measure the total energy of incoming particles. As the calorimeters are absorbing the particles they detect, any leptonic particle reaching the M2-5 muon detectors can be assumed to be a muon. Electrons and Photons are absorbed by the ECAL and any Tauons would have decayed long before reaching the far muon detectors.

<sup>1</sup>Radial distance from the beam pipe.

<sup>2</sup>Asumthal angle.

<sup>3</sup>The position at which the protons collided.

<sup>4</sup>The decay point of a short lived particle. i.e. B Meson.

## 1.4 LHCb Upgrade

### 1.4.1 VELO Upgrade

### 1.4.2 The Role of FPGA's in the VELO Upgrade

## 2 Scrambler

Due to radiation levels inside the detector chamber, the main data processing takes place in a concrete bunker away from the detector. To facilitate this, 20 optical links (per modul) are used to transfer the data from the front end VELO to the Data Acquisition FPGA (DAQ). When communicating data digitally, the transferring modul (TX) and the receiving modul (RX) must have synchronised clocks. In these case, the GWT serialiser is the TX, and the DAQ is the RX. When achieving synchronised clock, there are two main approaches:

I. Transmit the TX clock with the data to the RX modul - used in I<sup>2</sup>C and SPI communication.

II. Use bit-changes in the data to continuously synchronise the RX clock.

The former of these options, although widely used in conventional electronics, requires a finely tuned clock accounting for all possible delays. The latter, while negating cons of the former, requires data with a high density of transitions to reduce the likelihood of a desynchronisation event. Because delays in the data are possible, the latter option has been selected.

As it is necessary to ensure that the data has large density of transitions before being transmitted from the front-end detector to the DAQ modul. However, as the majority of super pixel hitmaps are empty, the data has a bias towards '0's. This reduces the frequency of transitions in the data - increasing the probability of a desynchronisation event. It is therefore necessary to scramble the data prior to transmission and descramble the data in the DAQ FPGA.

Scrambling and later descrambling the data is not a trivial exercise. The scrambling (TX) modul and descrambling (RX) modul must use a synchronised 'key', that is used in both the scrambling and descrambling processes. In the FPGA, the 'key' is derived from the previous states of the data. There are two methods when generating this 'key':

**Additive** The 'key' is generated by evolving the previous 'key' at each iteration of data using the incoming frame.

**Multiplicative** The 'key' is generated from the previous  $n$  frames. (Here  $n$  is a variable specific to the algorithm).

## 2.1 Scrambler Options

116 Three scrambling algorithms have been considered:

### Additive Scrambler

118 This scrambler is was originally implemented and used two sets of two-input XOR  
logic gates. As the name implies, this scrambler used additive key generation which  
120 is dependent all previous input frames since the last reset signal.

### Intermediate Scrambler

122 Created by Karol Hennessy, and deriving its name arbitrarily from the order of con-  
sideration, this multiplicative scrambler combines the current and previous frames  
124 to generate the *'key'*. Therefor, in the event of desynchronisation, only two frames are  
lost before the *'key'* is automatically recovered. This feature alone is a significant  
126 improvement over the Additive Scrambler.

### VeloPix Scrambler

128 This is the current implemented scramble algorithm in the DAQ and VeloPix code.  
Like the Intermediate Scrambler, it uses multiplicative *'key'* generation. However,  
130 the VeloPix scrambler is compatible with further constraints enforced by the ASIC,  
including the number of combinational logic operations. The Intermediate Scram-  
132 bler was design purely for simulation purposes and as such does not meet these  
constraints.

## 134 2.2 Cross Checks

The main priority when scrambling data, is ensuring that the data is recoverable. For all  
136 three scramblers, the algorithm was synthesised in Quartus<sup>2</sup> and simulated in Modelsim<sup>3</sup>.  
The aim of synthesising and simulating the scramblers in these programs was to ensure  
138 that the design was both physical in term of on-board logic gates, and to check that the  
scrambled data was recoverable, respectively.

140 Furthermore, a C++ simulation was created for the three scramblers. This simulation had  
two main purposes: firstly to cross check the output of the C++ against the Modelsim  
142 simulations; secondly to simulate the scrambler over a much larger simple of data as  
Modelsim simulations are less time effecient. In attition to the cross checks, the C++  
144 code allowed for the injection of a descronisation event, in which the *'key'* is lost. As  
expected, the Additive Scarmbler was unable to recover any data post descronisation,  
146 however the intermediate and VeloPix scarmblers both recovered the *'key'* after two  
frames and contiinoud to recover data.

## 2.3 Algorithm Analysis

For analytical purposes, it is assumed that fully scrambled data is indistinguishable from randomly generated data. For this reason, the three algorithms are not only tested against each other and the pre-scrambled QWT data but also randomly generated binary. The randomly generated data was created using the Python ‘*random*’ library, selecting a ‘0’ or ‘1’ with equal probability. While the Python ‘*random*’ library is only pseudo-random, on the scale of this example (i.e.  $\gg 100,000$  frames), it is by far sufficient.

A more mathematically rigorous approach, however, is to evaluate the system abstractly in the framework of statistical physics. In this abstraction, the 120 bit frame (with the header and parity removed) is considered an ensemble; microstates are the particular form of the frames; and macroscopic quantities can be calculated by averaging a large number of frames (i.e. the desync data). For the analysis outlined in section 2.3.1, predictions will be made using these principles and outlined in section 2.3.2.

In the context of the statistical model, it is reasonable to consider the degree of ‘*scrambledness*’ analogous to entropy. This analogy is not dissimilar to the common interpretation of entropy as a measure of disorder.

$$S \sim \ln(\Omega) \quad (2.1)$$

where  $\Omega$  is the number of microstates associated with the macrostate, we learn that this state of maximum entropy is a macrostate with the maximum number of associated microstates.

The entropic argument of Equation 2.1 is not only mathematically founded. For a scramble algorithm to hold for all possible data sets, it must also be capable of outputting all possible permutations. As such, assuming all possible outputs are equally likely, the count of each macroscopic output will be proportional to the number of microstates associated.

### 2.3.1 Measurements of the Algorithms

To compare the efficiency of the three algorithms in section 2.1, the algorithms were run over the same input data and compared for the following measures:

#### Number of Transitions Per Frame

This measure counts the total number of bit transitions (i.e.  $bit(n) \neq bit(n-1)$ ) in a 120 bit frame. The header and parity information was not included as they are not scrambled. This is an important test as one of the roles of the scrambler is to maximise the number of transitions.

#### Common Bit Chain Length

One of the downsides of the ‘Number of Transitions Per Frame’ analysis is that the two hypothetical 20 bit frames,



- a) 10101010101111111111,  
b) 10011001100110011001,

both with 10 transitions, are considered equaly. However, (b) is clearly a more suitable output for data transfer as (a) has a large probability of desynchronised due to the long chains of '1's in the right most bits. It is therefore also nessecary to evaluate the length of common bit chains within the scrambled data as shorter chains are more suitable for data transfer.

### Bit Asymetry

Pre-scramble, the data had a large bais towards '0's due to the majority of the hitmaps being empty. Scrambled data, via entropic arguments, *should* show zero bias eitherway. Therefor, by investigating how the number of '1's - '0's evolves over many frames, any bias in the scrambler can be found.

## 2.3.2 Statistical Predictions

### Number of Transitions Per Frame

Consider a particle in a symmetric, descrete time-dependent, two state system,

$$p_0(t) = p_1(t) = 0.5 \quad : \quad \forall t \in \mathbb{N}, \quad (2.2)$$

At each time itteration,

$$p_{i \rightarrow j}(t) = 0.5 \quad : \quad i, j = [0 \ 1], \quad \forall t \in \mathbb{N}. \quad (2.3)$$

However, assuming zero bias and detailed balance, as  $p_{1 \rightarrow 0}(t)$  is equal in both probalility and importance to  $p_{0 \rightarrow 1}(t)$ , the probability of a bit change shall herefore be refered to as  $p_t(t)$ .

Over a  $n$  step process, analogous to a  $n$  bit frame, the probalility distribution of the number of transitions  $N_t$  is given by Binomial statistics,

$$f(N_t) = \frac{n!}{N_t!(n - N_t)!} p^{N_t} (1 - p)^{n - N_t} \quad (2.4)$$

Simplified for the special case  $p = p_t = 0.5$ ,

$$f_t(N_t) = \frac{n!}{N_t!(n - N_t)!} (p_t)^n \quad (2.5)$$

For  $n = 120$ , we can calulate,

$$\langle N_t \rangle^{Binomial} = \sum_{N_t=0}^{n-1} N_t f(N_t) = n p_t = 60 \quad (2.6)$$

$$\sigma_{N_t}^{Binomial} = \sqrt{n p_t^2} = 5.48 \quad (2.7)$$

206 Furthermore, when considering the entropic argument in section 2.3 equation 2.1,  
 208 the number of microstates corespoding to each macrostate  $N_t$  can be related to  
 equation 2.5,

$$\Omega_t \sim \frac{n!}{N_t!(n - N_t)!} \quad (2.8)$$

$$< N_t >^{Entropic} = MAX[S_t] = MAX[\Omega_t] \quad (2.9)$$

This can be numerically solved,

$$< N_t >^{Entropic} = 60 \quad (2.10)$$

210 While the result of equation 2.10 does not contibute anything new, it is important  
 as a ‘*sanity check*’. Because the system can be described as in section 2.3, it would  
 212 indicated a problem in the theoretical framework if the result did not match.

### Common Bit Chain Length

214

The probability of a chain of length  $n$  is,

$$p_n = p_1(1 - p_t)^{n-1}, \quad : \quad n \in \mathbb{N}, \quad n > 1 \quad (2.11)$$

216 where  $p_1$  is the number of chains of lenght 1. As  $p_1 = N_0(1 - p_t)$ , where  $N_0$  is the  
 total number of chains,

$$\frac{N_n}{N_0} = (1 - p_t)^n, \quad : \quad n \in \mathbb{N}, \quad n > 1 \quad (2.12)$$

218 where  $N_n$  in the number of chains of length  $n$ . Takeing the log of both sides,

$$\begin{aligned} \log\left(\frac{N_n}{N_0}\right) &= n \log(1 - p_t), \\ \log(N_n) &= n \log(1 - p_t) + \log(N_0). \end{aligned} \quad (2.13)$$

220 Therefor, for a graph of  $\log(N_n)$  against  $n$  for a large sample of data, the gradient  
 would be  $\log(1 - p_t)$ . In this case, as  $p_t = 0.5$ ,

$$\log(1 - p_t) = -0.30 . \quad (2.14)$$

## Bit Asymetry

222

$A_{1,0}$ , the assymetry of ‘1’s and ‘0’s is defined as,

$$A_{1,0} = N_1 - N_0, \quad (2.15)$$

224

where  $N_1$  and  $N_0$  are the number of ‘1’s and ‘0’s respectively. We can consider the evolution of  $A_{1,0}$  with frame  $t$  of size  $n$  as a stockastic iterative map with zero deterministic growth [4],

226

$$A_{1,0}(nt + n \Delta t) = A_{1,0}(nt) + \mathcal{N}(nt) \quad (2.16)$$

Where  $\mathcal{N}$  is an independant random variable picked from a gaussian distribution. While  $A_{1,0}(t) \in \mathbb{Z}$ , in the limit of large  $nt$  we can approximate that  $A_{1,0}$  is continious.

228

If we consider the moments of  $A_{1,0}$ ,

$$\langle A_{1,0}(nt = M n \Delta t) \rangle = \sum_{m=0}^{M-1} \mathcal{N}(m n \Delta t), \quad (2.17)$$

$$\begin{aligned} \langle A_{1,0}(nt = M n \Delta t)^2 \rangle &= \sum_{m=0}^{M-1} \sum_{m'=0}^{M-1} \mathcal{N}(m n \Delta t) \mathcal{N}(m' n \Delta t) \delta_{mm'} \\ &= \sum_{m=0}^{M-1} \langle \mathcal{N}(m n \Delta t)^2 \rangle. \end{aligned} \quad (2.18)$$

230

Clearly, in Equation 2.17,  $\langle A_{1,0} \rangle = 0$ . In Equation 2.18, we assume the variance is of form  $(n \Delta t)^\alpha$  [4]. Then,

$$\langle A_{1,0}(nt = M n \Delta t)^2 \rangle = M(n \Delta t)^\alpha. \quad (2.19)$$

232

Running the analysis over the frames  $t = 0$  to  $t_f$ , the number of bits sampled is  $M = t_f/n \Delta t$ . Substituting this into Equation 2.19,

$$\langle A_{1,0}(nt = M n \Delta t)^2 \rangle = t_f (n \Delta t)^{\alpha-1}. \quad (2.20)$$

234

Concidering the three cases of  $\alpha$  in the approximation of continious  $n\Delta t$ :

- $\alpha > 1$ : Here  $A_{1,0} \rightarrow 0$  as  $\Delta t \rightarrow 0$ .
- $\alpha < 1$ : Here  $A_{1,0} \rightarrow \infty$  as  $\Delta t \rightarrow 0$ .
- $\alpha = 1$ : This is the only sensible choice.

236

238

With  $\alpha = 1$ ,

$$\langle A_{1,0}(nt = M n \Delta t)^2 \rangle = M(n \Delta t). \quad (2.21)$$

And thus,

$$\sigma_{A_{1,0}} = \sqrt{\langle A_{1,0}^2 \rangle - \langle A_{1,0} \rangle^2} = \sqrt{\langle A_{1,0}^2 \rangle} = \sqrt{n \Delta t}. \quad (2.22)$$

### 240 2.3.3 Results of Analysis

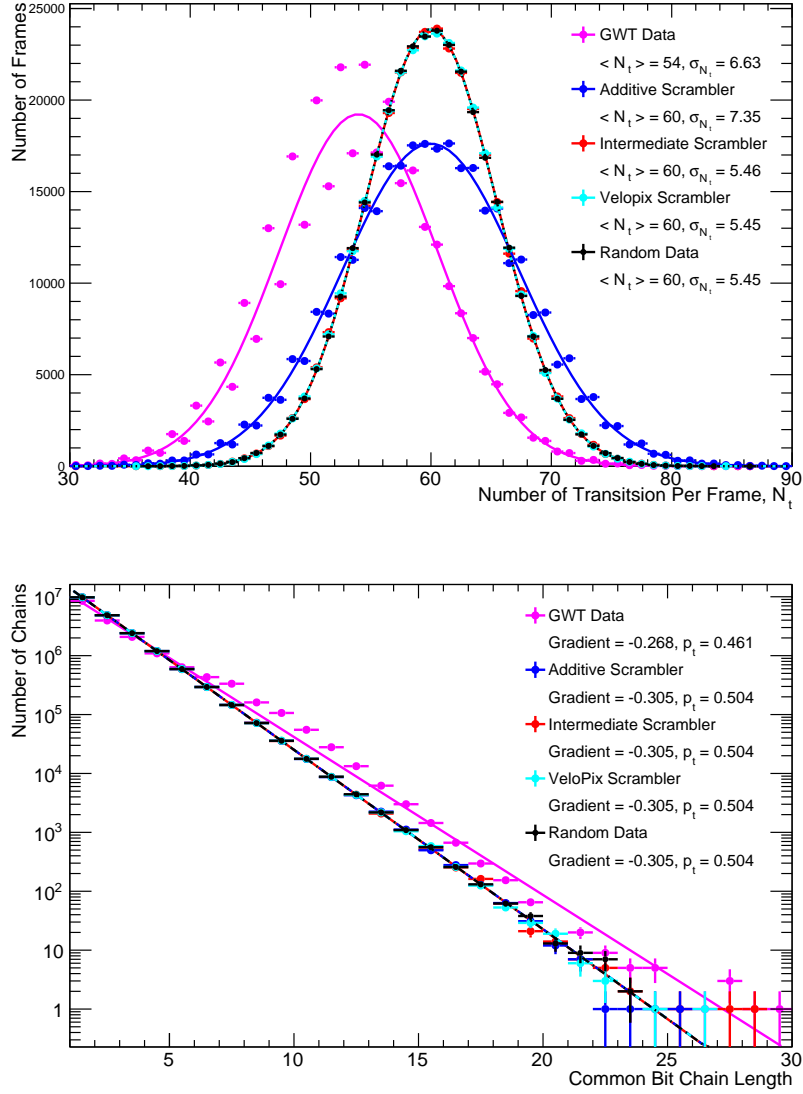


**Figure 2.1:** Results of the ‘*Number of Transitions Per Frame*’ analysis (Top) and the ‘*Common Bit Chain Length*’ analysis (Bottom). The results for the Random Data, Intermediate Scrambler and VeloPix Scrambler overlap for the ‘*Number of Transitions Per Frame*’ analysis. The results for the Random Data, Additive Scrambler, Intermediate Scrambler and VeloPix Scrambler approximately overlap for the ‘*Common Bit Chain Length*’ analysis.

The results from the ‘*Number of Transitions Per Frame*’ analysis, shown in Figure 2.1, show a strong correlation between the Intermediate and VeloPix Scramblers with the

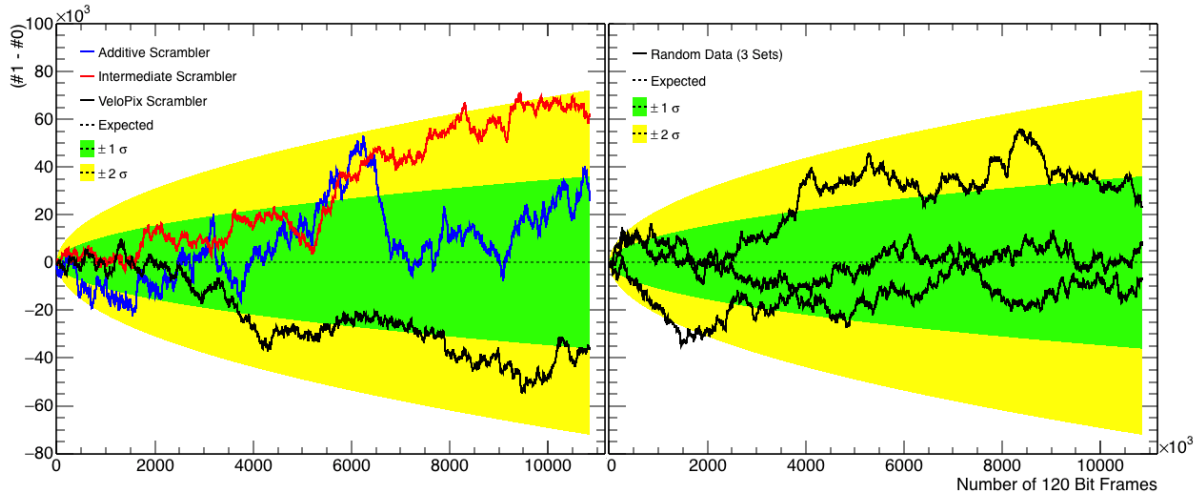


**Figure 2.2:** The results of the ‘*Bit Asymmetry*’ analysis.

randomly generated data. These results are within 1% agreement with the theoretical predictions for  $\langle N_t \rangle = 60$  and  $\sigma_{N_t} = 5.48$ , made in Section 2.3.2. The remarkable consistency between the theoretical predictions and the randomly generated data provides confidence in both the theory, and the scrambled nature of the Intermediate and VeloPix scrambler outputs.

All three scramblers, the random data, and the theoretical predictions are all consistent to within 1%. Comparing the two results for the Additive Scrambler, it is shown that while the frequency of longer chains is consistent with random data; but as the variance of transitions is larger than predicted, the long and short trains are more locally clustered.

The ‘*Bit Asymmetry*’ of each scrambler, shown in Figure 2.2, is consistent with the theoretical prediction. The deviation of  $A_{1,0}$  for the predicted mean of 0 is fully consistent with stochastic noise. The random data also shows consistency. This gives confidence in the assumptions made in Section 2.3.2.

One notable feature of Figure 2.2 is the steep gradient of the additive scrambler at  $t \sim 6 \cdot 10^6$ . However, as the data stays within the theoretical limits and the ‘*drop*’ is of approximately  $\Delta A_{1,0} \sim 60 \cdot 10^3$  over the range  $n \Delta t \sim 1.2 \cdot 10^8$  it would be difficult to construct any argument claiming that this feature is of statistical significance.

(I am tempted to run  $\chi^2$  analysis for a fit of  $y=0$  so show that the data is consistent with the model, but am not sure this will actually add to the argument?)

## 2.4 Conclusion

The consistency of random data and the theoretical predictions justifies the assumptions and approximations made in Section 2.3 and Section 2.3.2. Furthermore, the confirmation of the statistical model allows for accurate comparisons to be made from predicted

	$\langle N_t \rangle$	$\sigma_{N_t}$	Gradient	$p_t$
GQT data	54	6.63	-0.268	0.460
Additive Scrambler	60	7.35	-0.305	0.504
Intermediate Scrambler	60	5.45	-0.305	0.504
Velopix Scrambler	60	5.46	-0.305	0.504
Random Data	60	5.45	-0.305	0.504
Theoretical Prediction	60	5.48	-0.3	0.5

**Table 2.1:** The combined results of the algorithm analysis.

values and their measured counterparts.

The Additive Scrambler, while consistant with the ‘*Chain Length*’ and ‘*Bit Asymetry*’ analysis, has a variance in the transition frequency that leads the concultion that long and short chains are locally clusted. This is not ideal for data transfer. Many sequenchal long chains increase the probability of TX-RX clock desynchronisation. Furthermore, the additive scrambler will not recover from this loss of synchronisation, as the ‘*key*’ will never be recovered without a common reset signal.

The Intermediate Scrambler produced an output consistant with random data. This makes the algorithm suitable of data transfer. As already mentioned<sup>5</sup>, however, the scrambler is designed for computer simulated. As such, it is not suitable for implementation as it does not meet the additions requirments of the ASIC.

The VeloPix Scrambler, like the Intermediate Scrambler, produces a statistically scrambled output. Furthermore, the algorithm in inline with the additional requirments of the ASIC. As such, it ideal for implementation, and hense is currently the choice algorithm for use in the 2019 VELO upgrade.

---

<sup>5</sup>Note to Marco: this is in the scrabler options section

## References

- [1] Cern. *The Standard Model*. 2015. URL: <http://home.cern/about/physics/standard-model> (visited on 12/2015).
- [2] Altera. *Quartus Prime Software*. 2015. URL: <https://www.altera.com/products/design-software/fpga-design/quartus-prime/overview.html> (visited on 12/2015).
- [3] Mentor Graphics. *ModelSim - Leading Simulation and Debugging*. 2015. URL: <https://www.mentor.com/products/fpga/model/> (visited on 12/2015).
- [4] Kurt Jacobs. *Stochastic Processes for Physicists - Understanding Noisy Systems*. Cambridge University Press, 2010. ISBN: 9780521765428.